MATHEMATICAL BIOSCIENCES
AND ENGINEERING
Volume **15**, Number **5**, October **2018**

doi:10.3934/mbe.2018047

pp. **1055–1076**

MATHEMATICAL MODELLING OF CARDIAC PULSE WAVE REFLECTIONS DUE TO ARTERIAL IRREGULARITIES

Alexandre Cornet *

Imperial College London
South Kensington Campus, London SW72AZ, United Kingdom
&
Ecole normale supérieure Paris-Saclay
61 Avenue du Président Wilson, Cachan 94230, France

(Communicated by Yang Kuang)

Abstract. This research aims to model cardiac pulse wave reflections due to the presence of arterial irregularities such as bifurcations, stiff arteries, stenoses or aneurysms. When an arterial pressure wave encounters an irregularity, a backward reflected wave travels upstream in the artery and a forward wave is transmitted downstream. The same process occurs at each subsequent irregularity, leading to the generation of multiple waves. An iterative algorithm is developed and applied to pathological scenarios to predict the pressure waveform of the reflected wave due to the presence of successive arterial irregularities. For an isolated stenosis, analysing the reflected pressure waveform gives information on its severity. The presence of a bifurcation after a stenosis tends do diminish the amplitude of the reflected wave, as bifurcations' reflection coefficients are relatively small compared to the ones of stenoses or aneurysms. In the case of two stenoses in series, local extrema are observed in the reflected pressure waveform which appears to be a characteristic of stenoses in series along an individual artery. Finally, we model a progressive change in stiffness in the vessel's wall and observe that the less the gradient stiffness is important, the weaker is the reflected wave.

1. **Introduction.** Blood pressure is an important source of diagnostic information that can be used to detect and characterize cardiovascular diseases. Research has shown that studying the propagation of arterial pressure wave in the cardiovascular system leads to clinically useful information [12, 25, 13, 8, 14]. For example, the distensibility of an artery can be found from the speed of the pressure wave propagation in the vessel. Moreover, when a wave encounters an irregularity in the vessel, a transmitted and a reflected wave are generated from both sides of the irregularity [3, 22]. This is particularly important because reflected waves travel backward directly to the heart. These backward waves can apply an additional load on the muscle that is often seen as a risk factor for developing heart disease [11]. Research has shown that with age, due to the stiffening of the vessels and the presence of stenoses or aneurysms, reflected waves are more and more frequent [22]. Other studies were carried out to characterize the reflection coefficients of

2010 *Mathematics Subject Classification.* Primary: 15A24, 76D05; Secondary: 65F30.

Key words and phrases. Arterial irregularties, blood pressure, wave mechanics, mathematical modelling, iterative algorithm.

* Corresponding author: alexandre.cornet@ens-paris-saclay.fr.

irregularities such as stenoses [21] and to look at the effect of these irregularities on arterial pressure waves [2, 15].

In this research, we model arterial irregularities as local discontinuities in a geometric or mechanical property of the artery. The results apply to any local change in the area of the vessel, such as stenoses, aneurysms or bifurcations, and also apply to changes in other properties, such as the result of local stiffening with age due to plaques or remodelling of the arterial wall. Our model of arterial irregularities consists in an idealized system S_n, represented on Figure 1, which models a section of an artery, with n irregularities, modelled by discontinuities d_k, where $(k, n) \in \mathbb{N}^2$ and $1 \leq k \leq n$. The scope of this research is to study the effect of successive arterial irregularities modeled by system S_n on an incoming cardiac pulse wave P_i. To do so, we investigate on the resulting reflected pressure wave $P_{r,n}$ returning at the entrance of system S_n after the passing of the incoming cardiac pulse wave P_i. Thus, we introduce a measurement point, represented by point M at $x = 0$ on Figure 1, at which level we will numerically study the evolution of blood pressure.

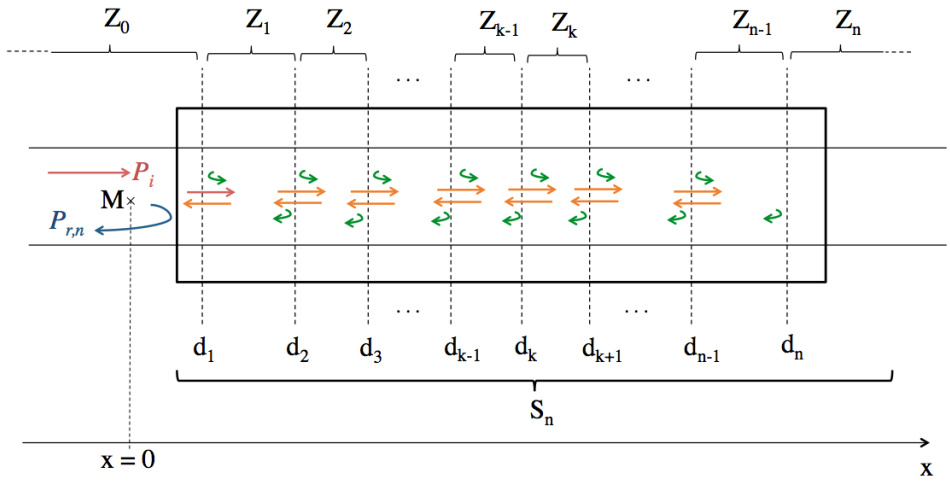

FIGURE 1. Graphical representation of the system with n discontinuities, S_n with $n \in \mathbb{N}$.

As represented on Figure 1, two successive discontinuities d_k and $d_k + 1$ delimit a zone Z_k in which the mechanical and geometric properties of the vessel are homogenous. Therefore, waves propagate in Z_k without any perturbation, until they reach either discontinuity d_{k+1}, the right delimitation of Z_k, for forward propagating waves, or discontinuity d_k, the left delimitation of Z_k, for backward propagating waves. When reaching a discontinuity, waves split into two components : a reflected pressure wave that is reflected within Z_k, represented by curled arrows on Figure 1, and a transmitted pressure wave that is transmitted in Z_{k-1} for backward traveling waves, or in Z_{k+1} for forward traveling waves, represented by straight arrows in Figure 1. Finally, P_i is the initially incoming wave that will be interfering with system S_n and that will be used as our input signal in this research. $P_{r,n}$ is the overall reflected pressure wave, that will return at the entrance of S_n after the passing of P_i in system S_n, which amplitude will be numerically estimated at the measurement point M in $x = 0$. Using the previous notation, S_0 represents a homogenous vessel, S_1 represents a single change, such as bifurcation and S_2 could be used to model a

stenosis or an aneurysm, where there is a section with different properties between two identical sections.

Hemodynamic studies, conducted with in vivo laboratory experiments [9, 1] have been used to test theoretical models, but nowadays, computers and simulations are more frequently used. Indeed, simulations allow us to access specific values such as the wall shear stress or the pressure distribution, which are difficult to extract from in vivo experiments [24, 20, 10, 19, 16]. Moreover, as invasive cardiovascular treatments are problematic, using simulations is particularly helpful to understand these diseases and to predict potential risks of medical complications [18]. Thus, a theoretical model that uses an iterative algorithm is developed in this paper, in order to study the effect of successive arterial irregularities on cardiac pulse waves. The iterative algorithm enables us to simulate the resulting reflected pressure wave at the entrance of S_n, at the measurement point M, at $x = 0$ on Figure 1, after the passing of the incident cardiac pulse wave denoted P_i. Finally, it is important to study the resulting reflected pressure wave returning at the entrance of S_n denoted $P_{r,n}$ as it is the backward reflected pressure wave traveling upstream directly to the heart. This backward wave can apply excessive pressure on the heart and is often seen as a risk factor for developing cardiovascular diseases. Moreover, knowing the waveform of $P_{r,n}$ could be useful for diagnostic purposes or for following treatment results.

2. Modelling cardiac pulse wave.

2.1. Governing equations.

We make the classical assumptions that the blood flow is incompressible, one-dimensional, inviscid, and we neglect gravity. Using these assumptions, the conservation of momentum is given by the Euler equation:

$$\rho\left(\frac{\partial U}{\partial t} + U\frac{\partial U}{\partial x}\right) = -\frac{\partial P}{\partial x}, \tag{2.1}$$

where U is the axial x-component of the blood velocity, P the blood pressure and ρ its density. By applying the mass conservation equation on a differentiable element of the blood vessel:

$$\frac{\partial A}{\partial t} = -\frac{\partial (AU)}{\partial x}, \tag{2.2}$$

where $A(x,t)$ is the local cross-sectional area of the differentiable element of the blood vessel, which is the cross-sectional area of the vessel at the considered x abscissa at time t. Finally, the classical tube law assumption [4, 5, 17, 14] expresses the local area as a function of pressure and position as:

$$\begin{cases} A(x,t) = A(P(x,t),x) \\ \frac{\partial A}{\partial P} > 0 \end{cases} \tag{2.3}$$

and is motivated by many empirical evidences [6, 7, 23]. Using the tube law (2.3), we can rewrite (2.2) in terms of P and U as:

$$\frac{\partial P}{\partial t} + U\frac{\partial P}{\partial x} + \frac{A}{A_P}\frac{\partial U}{\partial x} = -\frac{UA_x}{A_P}, \tag{2.4}$$

where:

$$A_x = \left.\frac{\partial A}{\partial x}\right|_P \quad \text{and} \quad A_P = \left.\frac{\partial A}{\partial P}\right|_x. \tag{2.5}$$

Expressing (2.1) and (2.2) in canonical matrix form:

$$\frac{\partial}{\partial t}\begin{pmatrix}P\\U\end{pmatrix}+\begin{pmatrix}U & \frac{A}{A_P}\\ \frac{1}{\rho} & U\end{pmatrix}\frac{\partial}{\partial x}\begin{pmatrix}P\\U\end{pmatrix}=\begin{pmatrix}-\frac{UA_x}{A_P}\\0\end{pmatrix}. \tag{2.6}$$

The eigenvalues of the matrix are $U \pm c$, where $c = \sqrt{1/\rho D}$ is the wave speed: the speed at which disturbances would propagate upstream and downstream in the absence of flow ($U = 0$). $D = A_P/A$ is the distensibility of the vessel that characterizes the vessel's capability of being distended or stretched. Since the eigenvalues are real, the system is hyperbolic and can be solved using the method of characteristics. Finally, from 1-D wave theory, we know that, when a wave encounters a discontinuity in a property of the medium in which it is propagating, it is reflected and transmitted on both sides of this discontinuity. In order to characterize the reflected and transmitted wave, we will use the reflection and transmission coefficients defined by:

$$\gamma = \frac{P_r}{P_i} \quad \text{and} \quad \lambda = \frac{P_t}{P_i}, \tag{2.7}$$

where P_i is the amplitude of the incident pressure wave, P_r the amplitude of the reflected pressure wave and P_t the amplitude of the transmitted pressure wave. These reflection and transmission coefficients are linked by the relation $\gamma + \lambda = 1$ [21]. This relation allows us to study the reflected pressure only as a function of reflection coefficient γ in the result section.

In this paper, we model two successive irregularities by two discontinuities d_k and d_{k+1} which delimit an homogeneous zone denoted Z_k as represented in Figure 1. A zone Z_k is fully characterized by its length $L_k = d_k - d_{k-1}$ and by its constant distensibility D_k. By convention, zone 0, Z_0 is the semi-infinite zone at the left of the first discontinuity d_1 of system S_n and zone n, Z_n is the semi-infinite zone at the right of the last discontinuity d_n of the system. The reflection and transmission coefficients at a discontinuity, defined above, depend on the direction of travel of the incident wave. In the following, a forward traveling wave in Z_k will interact with the discontinuity d_{k+1} to generate a backward reflected wave in Z_k with the reflection coefficient γ_{kk+1} and a forward transmitted wave in Z_{k+1} with the transmission coefficient λ_{kk+1}. Similarly, a backward wave in Z_k will interact with the discontinuity d_k generating a forward reflected wave in Z_k with the reflection coefficient γ_{kk-1} and a backward transmitted wave in Z_{k-1} with the transmission coefficient λ_{kk-1}. The time for a wave to propagate downstream through Z_k, from d_k to d_{k+1} is denoted T_k^+, and upstream through Z_k from d_{k+1} to d_k is denoted by T_k^- with :

$$T_k^+ = \frac{L_k}{c_k + U} = \frac{|d_k - d_{k-1}|}{\sqrt{1/\rho D_k} + U} \quad \text{and} \quad T_k^- = \frac{L_k}{c_k - U} = \frac{|d_k - d_{k-1}|}{\sqrt{1/\rho D_k} - U}. \tag{2.8}$$

Moreover, as the blood flow velocity is negligible compared to the celerity of pressure waves, we have $U/c_k \ll 1$, therefore :

$$T_k^{\pm} = \frac{L_k}{c_k \pm U} = \frac{L_k}{c_k\left(1 \pm \frac{U}{c_k}\right)} = \frac{L_k}{c_k\left(1 \pm \mathcal{O}\left(\frac{U}{c_k}\right)\right)}. \tag{2.9}$$

Under a zeroth-order approximation we can define a unique propagation time T_k for backward and forward traveling waves that is :

$$T_k = \frac{L_k}{c_k} = \frac{|d_k - d_{k-1}|}{\sqrt{1/\rho D_k}}. \tag{2.10}$$

Finally, All the properties for each zone Z_k are represented in this one quantity and, in the following, T_k will be used as our model input prescribed in the simulations when modelling different pathological scenarios in the results section. By convention, T_0 is the time for the wave to travel from measurement point M (at $x = 0$ in Z_0) to the first discontinuity d_1 of the system.

2.2. **Theoretical framework.** Assume $n \in \mathbb{N}$ and S_n is a system modelling the section of a vessel with n arterial discontinuities, and f is a continuous function on $[0, T]$ where $T \in \mathbb{R}_+$ modelling a realistic cardiac pulse wave. We want to know the resulting reflected pressure wave at the entrance of system S_n after the passing of a cardiac pulse wave. This resulting reflected pressure wave at the entrance of S_n is called the *response of system* S_n and is denoted $P_{r,n}$. In order to study the response of the S_n, we model the effect of the system as a functional denoted F_n that will be applied to the continuous function $f(t)$ modelling the incoming cardiac pulse wave on S_n, that is $P_{r,n} = F_n[f]$.

First we study the response of S_n when the incident wave is a single wavefront modelled by the Heaviside function. Since the governing system (2.5) is hyperbolic, wavefronts will be reflected and transmitted within the system and thus the resulting pressure at the entrance of the system is a superposition of shifted Heaviside functions with different amplitudes. In mathematical terms we write:

$$F_n[H](t) = \sum_{p=1}^{\infty} I_p H(t - t_p), \tag{2.11}$$

for all $n \in \mathbb{N}^*$ and $t \in \mathbb{R}_+$ and where I_p is the amplitude and t_p is the delay time of wave w_p.

In the case in which the incident wave is a continuous function f defined on $[0, T]$, we approximate f with f_m, where f_m is a superposition of Heaviside functions, for which $\lim_{m\to\infty} ||f - f_m||_\infty = 0$ which we define mathematically by:

$$\forall t \in [0, T] \;\; f_m(t) = \sum_{k=1}^{m} \alpha_k H(t - t'_k), \tag{2.12}$$

where $m \in \mathbb{N}$ and $m > 1$, $t'_k = (k-1)\frac{T}{m-1}$, $t'_m = T$, $\alpha_k = f\left(k\frac{T}{m-1}\right) - f\left((k-1)\frac{T}{m-1}\right)$, and $\alpha_m = f(T)$. As we mentioned, f_m converges uniformly towards f when m goes to infinity. Before each simulation, a convergence study is done in order to control the convergence of f_m towards f. In the results section we choose a value of $m = 10000$ for all simulations to ensure an appropriate convergence of the Heaviside approximation of the incident wave. The effect of the control parameter m on the computational solutions is discussed in the appendices.

From equation (2.8), by using the linearity and the continuity of the functional F_n and by using the expression of $F_n[H]$ from equation (2.7), we find:

$$F_n[f] = F_n\left[\lim_{m\to\infty} \sum_{k=1}^{m} \alpha_k H(t - t'_k)\right] = \lim_{m\to\infty} \sum_{k=1}^{m}\sum_{p=1}^{\infty} \alpha_k I_p H(t - t'_k - t_p). \tag{2.13}$$

Thus we focus on finding the unknowns I_p and t_p. In order to solve this problem we wrote an iterative algorithm that returns I_p and t_p for $p \in [\![1, N]\!]$, where $N \in \mathbb{N}$ is the number of iteration for which we consider the iterations have converged. The iterative algorithm that returns the unkowns I_p and t_p is explained in the

two following subsections. Before each simulation, a second convergence study is done in order to control the convergence of the iterative algorithm, and in order to choose the sufficient number of iterations for the algorithm to converge. To do so, we introduce a second control parameter ϵ that controls the difference between two iterations. We denote by $F_{n,N}[f]$ the result returned at the N^{th} iteration and $\Delta_r(F_N)$ the relative difference between $F_{n,N}[f]$ and $F_{n,N-1}[f]$. Mathematically the final number of iteration N for which the iterative algorithm has converged is such that:

$$\Delta_r(F_N) = \left\| \frac{F_{n,N}[f] - F_{n,N-1}[f]}{F_{n,N-1}[f]} \right\|_\infty = \left\| \frac{\lim\limits_{m\to\infty} \sum\limits_{k=1}^{m} \alpha_k I_N H\left(t - t'_k - t_N\right)}{\lim\limits_{m\to\infty} \sum\limits_{k=1}^{m} \sum\limits_{p=1}^{N-1} \alpha_k I_p H\left(t - t'_k - t_p\right)} \right\|_\infty < \epsilon \tag{2.14}$$

In the result section, we apply this method to physiological scenarios and choose $\epsilon = 0.1$ for each simulation to control the convergence of the algorithm. A senstitivity analysis regarding ϵ is detailed in the appendices.

2.3. **History of the waves.** In this section, we consider wavefronts propagating in system S_n and returning to the entrance, which are the waves that are transmitted from Z_1 to Z_0. The history of a particular wave can be written in different but equivalent ways: the sequence of zones traversed, the sequence of discontinuities encountered or, most conveniently for our purposes, the sequence of reflections/transmissions that the wave has undergone. Indeed, a wavefront propagating in the system is fully characterized by its list of reflection and transmission coefficients of all the reflection and transmission it went through at each discontinuity d_k within the system. For wave w_p, its reflection/transmission coefficient list is denoted as $\widetilde{w_p}$ in the following, often called "the history of wave w_p". We illustrate S_3, the system with three discontinuities, in Figure 2.

In the (x,t)-diagram plotted in Figure 2, vertical dashed lines represent the borders of the different homogenous zones, delimited by the discontinuities of the system, while diagonal lines represent the different paths of the waves traveling within the system. The slope of the diagonal lines is constant within a homogenous zone, and is equal to the speed of propagation of a wave through this zone.

We consider returning wavefronts in the (x,t)-diagram of Figure 2 and write down their respective reflection/transmission coefficient list as examples. The returning wavefront w_1 at time $t = 2T_0$ has only been reflected on Z_1 coming from Z_0. Its list is $\widetilde{w_1} = (\gamma_{01})$. The returning wavefront w_2 at time $t = 2T_0 + 2T_1$ has been transmitted from Z_0 to Z_1 through d_1, reflected at Z_2 while in Z_1 and finally transmitted back to Z_0 from Z_1 through d_1. Its list is $\widetilde{w_2} = (\lambda_{01}, \gamma_{12}, \lambda_{10})$. The returning wavefront w_3 at time $t = 2T_0 + 4T_1$ has the same history as the previous wavefront, except it is reflected two more times in Z_1: at Z_0 the first time and at Z_2 the second time. Thus, its list is $\widetilde{w_3} = (\lambda_{01}, \gamma_{12}, \gamma_{10}, \gamma_{12}, \lambda_{10})$. Using the same notation, the returning wavefront w_4 at time $t = 2T_0 + 2T_1 + 2T_2$ has the list $\widetilde{w_4} = (\lambda_{01}, \lambda_{12}, \gamma_{23}, \lambda_{21}, \lambda_{10})$, and so on.

If we know the history of a wavefront returning at the measurement point M at $x = 0$ then we know the time of arrival and amplitude of the wave. Indeed, for instance, according to the definition of the reflection and transmission coefficients (2.6), if we consider the wavefront w_1 that is directly reflected on discontinuity d_1 between Z_1 and Z_2, it returns to the measurement point with the amplitude γ_{01} and

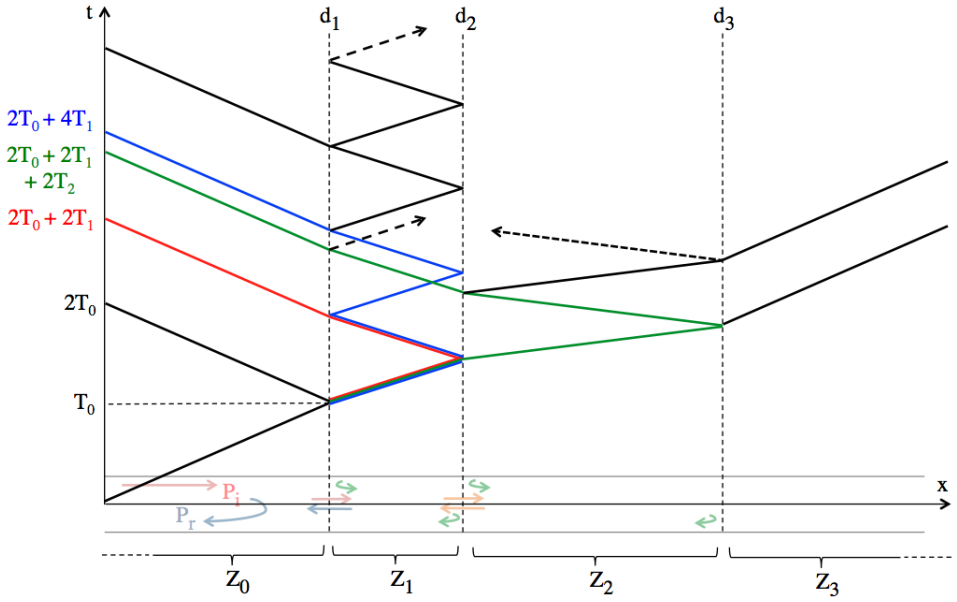

FIGURE 2. (x,t)-diagram of the system with 3 discontinuities, S_3.

it took $2T_0$ to return as it traveled back and forth into Z_0. Similarly, wavefronts that are transmitted through d_1 from Z_0 to Z_1 has their amplitude firstly multiplied by λ_{01}, and if we consider the wavefront w_2 that is then reflected on d_2 between Z_1 and Z_2, and then transmitted back through d_1 from Z_1 to Z_0, its amplitude is therefore multiplied by the reflection coefficient between Z_1 and Z_2 which is γ_{12} and then by the transmission coefficient from Z_1 and Z_0 which is λ_{10}. Thus, the amplitude of the returning wavefront w_2 is given by the product $I_2 = \lambda_{01} \cdot \gamma_{12} \cdot \lambda_{10}$, and its time of return is the summation of the different back and forth traveling times through Z_0 and Z_1 that is $t_2 = T_0 + T_1 + T_1 + T_0 = 2T_0 + 2T_1$. Therefore, the history of the wavefronts enables us to find t_p and I_p for any wavefront w_p. Indeed, according to the definition of the reflection and transmission coefficients, if we know the lists $\widetilde{w_p}$ of reflection/transmission coefficients of any returning wavefront w_p, then we know its amplitude as it is given by:

$$\forall p \in [\![1, N]\!], \quad I_p = \prod_{\substack{(i,j,k,l) \\ \lambda_{ij} \in \widetilde{w_p} \\ \gamma_{kl} \in \widetilde{w_p}}} \lambda_{ij} \cdot \gamma_{kl}, \tag{2.15}$$

Moreover, the time for a wavefront to return is, by definition, and as we saw in the previous examples, the summation of the different back and forth traveling times the wave goes through in the system before returning. Therefore, this can be mathematically defined as:

$$\forall p \in [\![1, N]\!], \quad t_p = \sum_{\substack{(i,j) \\ \lambda_{ij} \in \widetilde{w_p} \\ \gamma_{ij} \in \widetilde{w_p}}} T_i, \tag{2.16}$$

where N is the number of iterations.

In this research, we developed an iterative algorithm returning all the lists $\widetilde{w_p}$ which enables us to compute I_p and t_p for any wave w_p and thus determine $P_{r,n}$. The method is explained in the following section. Then, this algorithm will be applied to different physiological scenarri that are presented with the computational solutions in the results section.

3. **Method.**

3.1. **Explaining the algorithm for 3 discontinuities,** $n = 3$**.** The algorithms for determining the lists $\widetilde{w_p}$ for S_1 and S_2 are too simple to indicate how to develop an algorithm for systems with more discontinuities. The study of a system with 3 discontinuities, S_3, however is not trivial and does provide us with a method that can be generalized to larger systems. Thus, the study of system S_3 with three discontinuities ($n = 3$) is important because we will see how from the study of this system we can easily have the response for any other systems with any number of discontinuities. An illustration of S_3 is given in Figure 2. We study the first reflection/transmission coefficient lists of the wavefronts that are returning the entrance of system S_3. We stored the lists by their lengths (*i.e*: the number of elements in the list, which is the number of reflection and transmission coefficients) into matrices. The matrices are denoted $M_{n,l}$ where n is the number of discontinuities of system S_n and l the length of the coefficients lists of the matrix (thus the number of columns of the matrix). We first noticed that the length of a list, l, can only be an odd number for the wavefront to return at the entrance of the system. We were able to write down manually the first five matrices of the returning wavefronts:

$$M_{3,1} = \begin{pmatrix} \gamma_{01} \end{pmatrix},$$

$$M_{3,3} = \begin{pmatrix} \lambda_{01} & \gamma_{12} & \lambda_{10} \end{pmatrix},$$

$$M_{3,5} = \begin{pmatrix} \lambda_{01} & \gamma_{12} & \gamma_{10} & \gamma_{12} & \lambda_{10} \\ \lambda_{01} & \lambda_{12} & \gamma_{23} & \lambda_{21} & \lambda_{10} \end{pmatrix},$$

$$M_{3,7} = \begin{pmatrix} \lambda_{01} & \gamma_{12} & \gamma_{10} & \gamma_{12} & \gamma_{10} & \gamma_{12} & \lambda_{10} \\ \lambda_{01} & \gamma_{12} & \gamma_{10} & \lambda_{12} & \gamma_{23} & \lambda_{21} & \lambda_{10} \\ \lambda_{01} & \lambda_{12} & \gamma_{23} & \lambda_{21} & \gamma_{10} & \gamma_{12} & \lambda_{10} \\ \lambda_{01} & \lambda_{12} & \gamma_{23} & \gamma_{21} & \gamma_{23} & \lambda_{21} & \lambda_{10} \end{pmatrix},$$

and,

$$M_{3,9} = \begin{pmatrix} \lambda_{01} & \gamma_{12} & \gamma_{10} & \gamma_{12} & \gamma_{10} & \gamma_{12} & \gamma_{10} & \gamma_{12} & \lambda_{10} \\ \lambda_{01} & \gamma_{12} & \gamma_{10} & \gamma_{12} & \gamma_{10} & \lambda_{12} & \gamma_{23} & \lambda_{21} & \lambda_{10} \\ \lambda_{01} & \gamma_{12} & \gamma_{10} & \lambda_{12} & \gamma_{23} & \lambda_{21} & \gamma_{10} & \gamma_{12} & \lambda_{10} \\ \lambda_{01} & \gamma_{12} & \gamma_{10} & \lambda_{12} & \gamma_{23} & \gamma_{21} & \gamma_{23} & \lambda_{21} & \lambda_{10} \\ \lambda_{01} & \lambda_{12} & \gamma_{23} & \lambda_{21} & \gamma_{10} & \gamma_{12} & \gamma_{10} & \gamma_{12} & \lambda_{10} \\ \lambda_{01} & \lambda_{12} & \gamma_{23} & \lambda_{21} & \gamma_{10} & \lambda_{12} & \gamma_{23} & \lambda_{21} & \lambda_{10} \\ \lambda_{01} & \lambda_{12} & \gamma_{23} & \gamma_{21} & \gamma_{23} & \lambda_{21} & \gamma_{10} & \gamma_{12} & \lambda_{10} \\ \lambda_{01} & \lambda_{12} & \gamma_{23} & \gamma_{21} & \gamma_{23} & \gamma_{21} & \gamma_{23} & \lambda_{21} & \lambda_{10} \end{pmatrix}.$$

We build larger matrices iteratively using submatrices from previous matrices. We consider the matrix $A_n \in \mathcal{M}_{n,3}$ with n identical rows equal to $(\lambda_{01}, \gamma_{12}, \gamma_{10})$, the matrix $B_n \in \mathcal{M}_{n,4}$ with n identical rows equal to $(\lambda_{01}, \lambda_{12}, \gamma_{23}, \lambda_{21})$ and the matrix $C_n \in \mathcal{M}_{n,4}$ with n identical rows equal to $(\lambda_{01}, \lambda_{12}, \gamma_{23}, \gamma_{21})$. We now define the matrices $M_{3,7}^{[1]}$ which is equal to $M_{3,7}$ with its first column removed and $M_{3,7}^{[1,2]}$ which

is equal to $M_{3,7}$ with its first and second columns removed. Thus, we can express $M_{3,9}$ as:

$$M_{3,9} = \begin{pmatrix} A_4 & M_{3,7}^{[1]} \\ B_2 & M_{3,7}^{[1,2]} \\ C_2 & \end{pmatrix}.$$

Furthermore, we show by induction that for any $p > 3$:

$$M_{3,2p+1} = \begin{pmatrix} A_{2^{p-2}} & M_{3,2p-1}^{[1]} \\ B_{2^{p-3}} & M_{3,2p-1}^{[1,2]} \\ C_{2^{p-3}} & \end{pmatrix}.$$

Thus we develop an iterative algorithm that is able to generate automatically all the matrices, thus all the reflection/transmission coefficient lists of the returning wavefronts, stored in the matrices. From these coefficient lists, we can easily get the values of the unknowns I_p and t_p using equation (2.10) and equation (2.11). By doing so, the problem is solved for system S_3 with three discontinuities. Moreover, both system S_1 with one discontinuity and S_2 with two discontinuities are also solved. Indeed, S_1 (resp. S_2) is only a particular cases of S_3 for which the reflection and transmission coefficients γ_{12}, γ_{23} and λ_{12}, λ_{23} (resp. γ_{23} and λ_{23}) are equal to 0.

3.2. **Extending the algorithm from 3 discontinuities to 4 discontinuities, $n = 3$ to $n = 4$.** Reflection/transmission coefficients lists for S_3 also represent returning waves in S_4. Any additions to the lists in S_4 compared to the one with S_3 occur because the wavefront reached d_4. With the presence of the discontinuity d_4 in S_4, wavefronts can now be transmitted through d_3 and still be returning at the entrance of S_4 if reflected on d_4. System S_4 is illustrated in Figure 3.

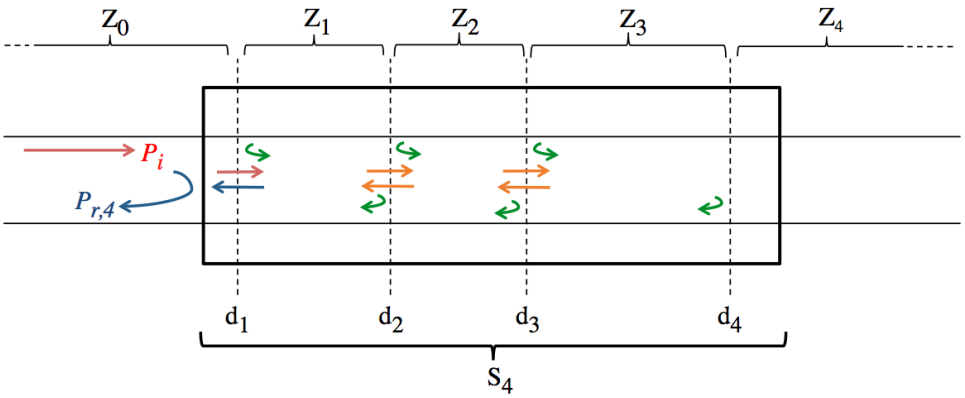

FIGURE 3. Graphical representation of the system with 4 discontinuities, S_4.

When a wavefront is transmitted through d_3 in zone Z_3, a returning wavefront will be transmitted back to Z_2 after an odd number of reflections in Z_3. Finally, a returning wavefront for S_4 cannot be transmitted through d_4 as there are no more discontinuities after d_4 to be reflected on.

This idea was transplanted into the algorithm. For a wavefront to be propagating in Z_2 in the positive x-direction, its last reflection and transmission were either the reflection from in Z_2 on d_2 or the transmission from Z_1 to Z_2 through d_2. This means that the last term of its wave history is either γ_{21} or λ_{12}. In order to generate all the new coefficient lists of the returning wavefronts for S_4 from the previously generated matrices for S_3 we simply have to add to any lists containing γ_{21} or λ_{12} in the matrices of S_3 the following sequence of coefficients due to:

- The transmission from Z_2 to Z_3 through d_3: λ_{23}.
- The odd number of reflection in Z_3 on d_3 and d_4: $(...\gamma_{34}, \gamma_{32}, ..., \gamma_{34}, \gamma_{32}, ..., \gamma_{34}, \gamma_{32}, \gamma_{34}, ...)$.
- The final transmission from Z_3 to Z_2 through d_3: λ_{32}.

We finally have analogous matrices from the one obtained in the previous study of S_3 with additional lines, written in bold in the following, due to the presence of the new discontinuity d_4:

$$M_{4,1} = \begin{pmatrix} \gamma_{01} \end{pmatrix},$$

$$M_{4,3} = \begin{pmatrix} \lambda_{01} & \gamma_{12} & \lambda_{10} \end{pmatrix},$$

$$M_{4,5} = \begin{pmatrix} \lambda_{01} & \gamma_{12} & \gamma_{10} & \gamma_{12} & \lambda_{10} \\ \lambda_{01} & \lambda_{12} & \gamma_{23} & \lambda_{21} & \lambda_{10} \end{pmatrix},$$

$$M_{4,7} = \begin{pmatrix} \lambda_{01} & \gamma_{12} & \gamma_{10} & \gamma_{12} & \gamma_{10} & \gamma_{12} & \lambda_{10} \\ \lambda_{01} & \gamma_{12} & \gamma_{10} & \lambda_{12} & \gamma_{23} & \lambda_{21} & \lambda_{10} \\ \lambda_{01} & \lambda_{12} & \gamma_{23} & \lambda_{21} & \gamma_{10} & \gamma_{12} & \lambda_{10} \\ \lambda_{01} & \lambda_{12} & \gamma_{23} & \gamma_{21} & \gamma_{23} & \lambda_{21} & \lambda_{10} \\ \boldsymbol{\lambda_{01}} & \boldsymbol{\lambda_{12}} & \boldsymbol{\lambda_{23}} & \boldsymbol{\gamma_{34}} & \boldsymbol{\lambda_{32}} & \boldsymbol{\lambda_{21}} & \boldsymbol{\lambda_{10}} \end{pmatrix},$$

and,

$$M_{4,9} = \begin{pmatrix} \lambda_{01} & \gamma_{12} & \gamma_{10} & \gamma_{12} & \gamma_{10} & \gamma_{12} & \gamma_{10} & \gamma_{12} & \lambda_{10} \\ \lambda_{01} & \gamma_{12} & \gamma_{10} & \gamma_{12} & \gamma_{10} & \lambda_{12} & \gamma_{23} & \lambda_{21} & \lambda_{10} \\ \lambda_{01} & \gamma_{12} & \gamma_{10} & \lambda_{12} & \gamma_{23} & \lambda_{21} & \gamma_{10} & \gamma_{12} & \lambda_{10} \\ \lambda_{01} & \gamma_{12} & \gamma_{10} & \lambda_{12} & \gamma_{23} & \gamma_{21} & \gamma_{23} & \lambda_{21} & \lambda_{10} \\ \lambda_{01} & \lambda_{12} & \gamma_{23} & \lambda_{21} & \gamma_{10} & \gamma_{12} & \gamma_{10} & \gamma_{12} & \lambda_{10} \\ \lambda_{01} & \lambda_{12} & \gamma_{23} & \lambda_{21} & \gamma_{10} & \lambda_{12} & \gamma_{23} & \lambda_{21} & \lambda_{10} \\ \lambda_{01} & \lambda_{12} & \gamma_{23} & \gamma_{21} & \gamma_{23} & \lambda_{21} & \gamma_{10} & \gamma_{12} & \lambda_{10} \\ \lambda_{01} & \lambda_{12} & \gamma_{23} & \gamma_{21} & \gamma_{23} & \gamma_{21} & \gamma_{23} & \lambda_{21} & \lambda_{10} \\ \boldsymbol{\lambda_{01}} & \boldsymbol{\gamma_{12}} & \boldsymbol{\gamma_{10}} & \boldsymbol{\lambda_{12}} & \boldsymbol{\lambda_{23}} & \boldsymbol{\gamma_{34}} & \boldsymbol{\lambda_{32}} & \boldsymbol{\lambda_{21}} & \boldsymbol{\lambda_{10}} \\ \boldsymbol{\lambda_{01}} & \boldsymbol{\lambda_{12}} & \boldsymbol{\lambda_{23}} & \boldsymbol{\gamma_{34}} & \boldsymbol{\lambda_{32}} & \boldsymbol{\lambda_{21}} & \boldsymbol{\gamma_{10}} & \boldsymbol{\gamma_{12}} & \boldsymbol{\lambda_{10}} \\ \boldsymbol{\lambda_{01}} & \boldsymbol{\lambda_{12}} & \boldsymbol{\lambda_{23}} & \boldsymbol{\gamma_{34}} & \boldsymbol{\lambda_{32}} & \boldsymbol{\gamma_{21}} & \boldsymbol{\gamma_{23}} & \boldsymbol{\lambda_{21}} & \boldsymbol{\lambda_{10}} \\ \boldsymbol{\lambda_{01}} & \boldsymbol{\lambda_{12}} & \boldsymbol{\gamma_{23}} & \boldsymbol{\gamma_{21}} & \boldsymbol{\lambda_{23}} & \boldsymbol{\gamma_{34}} & \boldsymbol{\lambda_{32}} & \boldsymbol{\lambda_{21}} & \boldsymbol{\lambda_{10}} \\ \boldsymbol{\lambda_{01}} & \boldsymbol{\lambda_{12}} & \boldsymbol{\lambda_{23}} & \boldsymbol{\gamma_{34}} & \boldsymbol{\gamma_{32}} & \boldsymbol{\gamma_{34}} & \boldsymbol{\lambda_{32}} & \boldsymbol{\lambda_{21}} & \boldsymbol{\lambda_{10}} \end{pmatrix}.$$

4. **Results for a half-sinusoidal model of a cardiac pulse wave.** In the following section, we are going to look at the reflected pressure versus time $P_{r,n}(t)$ at the entrance of systems with different numbers of discontinuities, when the incident pressure wave is modeled by a half-sinusoidal wave : $P_i(t) = \sin(\pi t/0.1)$. We will

consider cases of 1, 2, 3 and 4 discontinuities in the system. Each study is directly linked to common physiological scenarios. The results are given by simulations obtained with the previously explained algorithm and after a convergence study done on the two control parameters. We chose in the following simulations $m = 10000$ and $\epsilon = 0.1$ as explained in the theoretical framework. Detailed sensitivity studies regarding the values of the control parameters m and ϵ are given in the appendices for cases with $n = 2$, $n = 3$ and $n = 4$.

4.1. **Results for one discontinuity (n =1): Application to a bifurcation or an abrupt change in stiffness.** Applying the algorithm to system S_1 can be useful to model a bifurcation or an abrupt change in the vessel's stiffness as both can be modelled with a system with only one discontinuity. We looked at the results for different values of reflection coefficients and saw that the results obtained from the algorithm matched with the trivial analytical solution $P_{r,1}(t) = \gamma_{01} P_i(t) = \gamma_{01} \sin(\pi t/0.1)$. This comparison allowed us test and valid the algorithm on this example.

4.2. **Results for two discontinuities (n = 2): Application to an isolated stenosis or an isolated aneurysm.** In this section we apply the algorithm to system S_2, the system with two irregularities. This is particularly useful to model isolated stenoses or isolated aneurysms. Indeed, these pathologies can be modelled by two successive changes in the vessel's area as the flow undergoes a narrowing which induces a discontinuity in the local area. On Figure 4 are gathered the results of the simulations modelling the reflected pressure at the entrance of an isolated stenosis for different severities by changing the values of the reflection coefficients γ_{01} and γ_{12}. In this particular example, we were able to derive an analytical solution of the reflected pressure (see appendix 6.1). We compared the analytical solution with the results returned by the algorithm by plotting the analytical solution in dashed line on Figure 4 for $\gamma_{01} = \gamma_{12} = 0.8$. We see that the analytical (dashed lines) and the computational responses match, which validates once more the algorithm. The fact that the analytical and the computational solutions are not identical is due to the degree of convergence of the iterations controlled by the parameter ϵ. As $\epsilon \longrightarrow 0$, the computational solution uniformly converges towards the analytical solution as we can see on Figure 12 in the appendices, but computation times increase rapidly. Fixing the value of ϵ was done by choosing the right balance between computation times and the exactness of the computational solutions. In our simulations, we fixed $\epsilon = 0.1$ because computations are executed fast enough to investigate on different scenarios and we are satisfied of the precision of the computational solutions returned by the algorithm. In these simulations we chose as input parameters : $T_0 = 1$ ms and $T_1 = 0.5$ ms, which corresponds to a 5 mm long stenosis.

4.3. **Results for three discontinuities ($n = 3$): Application to a stenosis followed by a bifurcation.** For a number of discontinuities strictly greater than 2 ($n > 2$), there are no general analytical solution. This justifies our need to develop the iterative algorithm. Applying the algorithm on system S_3 can be helpful to study the influence of a bifurcation downstream a stenosis. As bifurcations have commonly low reflection coefficients we fix at 0.05 the value of the bifurcation's reflection coefficient. On Figure 5 are gathered the simulated reflected pressure waveforms at the entrance of system S_3 modelling stenoses with different degrees of severity followed by a bifurcation. In these simulations we chose as input parameters: $T_0 =$

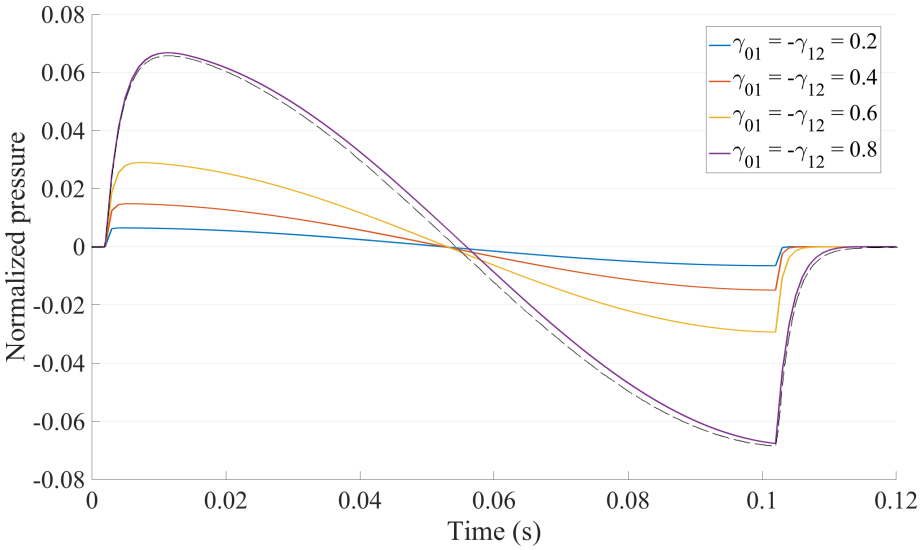

FIGURE 4. Normalized reflected pressure versus time at the entrance of a 5 mm long stenosis modelled with S_2, with different values of reflection coefficients.

1 ms, $T_1 = 0.5$ ms and $T_2 = 6$ ms which corresponds to a 5 mm long stenosis followed by a bifurcation 6 cm downtream. We notice that the amplitude of the reflected pressure waveform for all scenarios is around 0.05 except for the case $\gamma_{01} = 0.8$. This means that for $0 \leq \gamma_{01} \leq 0.6$, the amplitude of the incident pressure wave is multiplied by the value of the bifurcation's reflection coefficient. Moreover, we observe a local minima in pressure near $t = 100$ ms for all scenarios, except for the case $\gamma_{01} = 0$ which is the case equivalent to no upstream stenosis. This let us think that this peak is due to the presence of the upstream stenosis as we can also see on Figure 4 the waveform for an isolated stenosis reaching its minimal values near $t = 100$ ms.

4.4. **Results for four discontinuities (n = 4).**

4.4.1. *Application to two stenoses in series.* Modelling the reflected pressure waveform upstream two stenoses in series is particularly useful because in some cases, one stenosis can hide a second downstream stenosis. This can easily be modelled using S_4, the system with four discontinues because two stenoses in series can be seen as four successive discontinuities in the vessel's area. We fix the reflection coefficients corresponding to the dowstream stenosis and vary the coefficients of the first stenosis to investigate different scenarios. Results are gathered on Figure 6. For these simulations, we chose as input parameters: $T_0 = 1$ ms, $T_1 = 0.5$ ms, $T_2 = 6$ ms and $T_3 = 0.5$ ms which corresponds to a first 5 mm long stenosis spaced 6 cm away from a second 5 mm stenosis downstream. The main difference with the case of one isolated stenosis is the presence of local extrema observed on the returning pressure waveform. A local minimum is observed at time $t = 16$ ms that matches with the time for a single wavefront to reach the downstream stenosis and to return back to

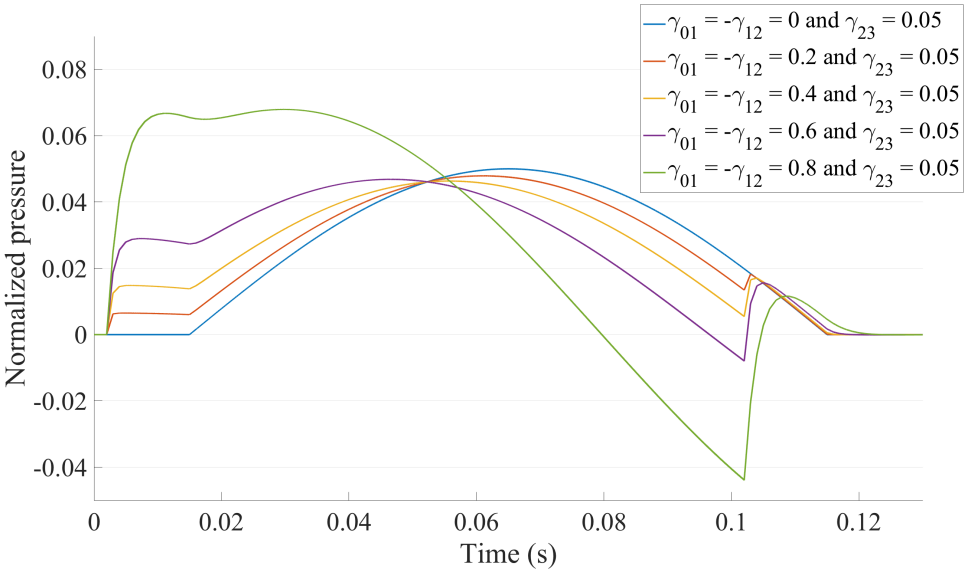

FIGURE 5. Normalized reflected pressure versus time at the entrance of a 5 mm long stenosis, 6 cm before a bifurcation modelled with S_3, with different values of reflection coefficients for the upstream stenosis and a constant reflection coefficient for the bifurcation.

where the pressure is recorded. We suppose that this local minimum is due to the presence of the downstream stenosis as it was not observed in the case of an isolated stenosis. Observing such local extrema in the reflected pressure waveform could be helpful to detect stenoses in series and could have important clinical implications explained in the discussion section.

4.4.2. *Application to smooth changes in vessel's stiffness.* Modelling an abrupt change in stiffness was done with $n = 1$ discontinuity using S_1. However, one could expect, in some cases, the changes in stiffness along an artery to occur relatively smoothly. A smooth transition can be modelled by discretizing the progressive change in the arterial property with several local discontinuities in the arterial stiffness. This number of discontinuities depends on how one discretizes this progressive change. The more discontinuities you consider, the better will be the discretization. In our case, we model a smooth change in stiffness by discretizing this progressive change with four localized discontinuities in stiffness that are characterized by their relative reflection coefficients. To do so, we consider system S_4 with four discontinuities that all have the same relative reflection coefficients γ and for which the propagation times of the pressure wave to travel between two successive discontinuities are the same and are equal to a parameter denoted ΔT on Figure 7. ΔT is directly related to the gradient of stiffness of the artery and can physically describe how smooth is the change in the vessel's property. The more ΔT is important, the more the discontinuities are spaced and thus, the less the gradient in stiffness of the artery is important as the different reflection coefficients are fixed and equal to γ. On Figure 7 are gathered results of simulations for which we consider the four reflection coefficients fixed and equal to $\gamma = 0.1$ and where we study the effect

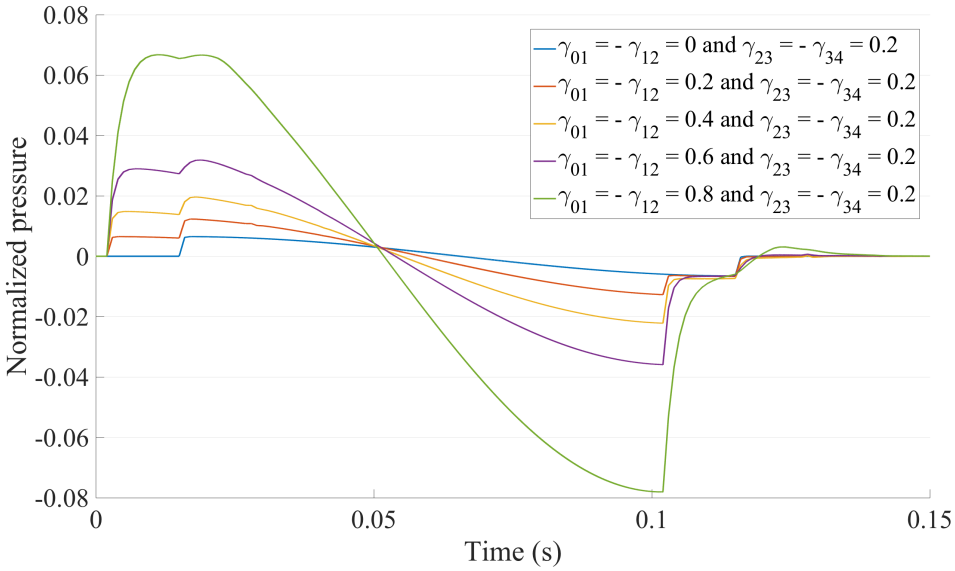

FIGURE 6. Normalized reflected pressure versus time at the entrance of two 5 mm stenoses in series modelled with S_4, with different value of reflection coefficients for the upstream stenosis and constant reflection coefficients for the downstream stenosis.

of ΔT on the reflected pressure waveform. In our case we observe that the more ΔT is important, the less the amplitude of the reflected wave is important. This means that the amplitude of the reflected pressure wave decreases with the stiffness gradient as we could physically expect. Interpretations of this result are gathered in the discussion section.

5. **Discussion and conclusion.** This research presents a method that allows clinicians to have qualitative predictions of the resulting reflected pressure waveform upstream a series of successive arterial irregularities. The iterative algorithm developed in this paper is used to model different clinical scenarios and simulate the effect of arterial irregularities, such as stenoses or arterial stiffening, on the pressure waveform. The results we obtained for a single stenosis with the algorithm were compared with the analytical solution developed in the appendix. This comparison allowed us to test the robustness of the algorithm and validate the method we use in this research. The algorithm is applied on more complicated physiological cases than isolated stenoses, such as a stenosis followed by a bifurcation. In that case, the global amplitude of the pressure is multiplied by the reflection coefficient of the downstream bifurcation. Usually, the reflection coefficients of bifurcations are relatively small, around 0.05. Measuring normalized reflected pressure wave with small amplitudes could indicate clinicians the presence of a bifurcation near the measurement point.

We also applied our method to two stenoses in series, which could prevent a stenosis hiding a second downstream stenosis during diagnosis, meaning that only the first stenosis is treated and potentially necessitating a second operation. If clinicians were able to detect directly both stenosis, only one operation would be

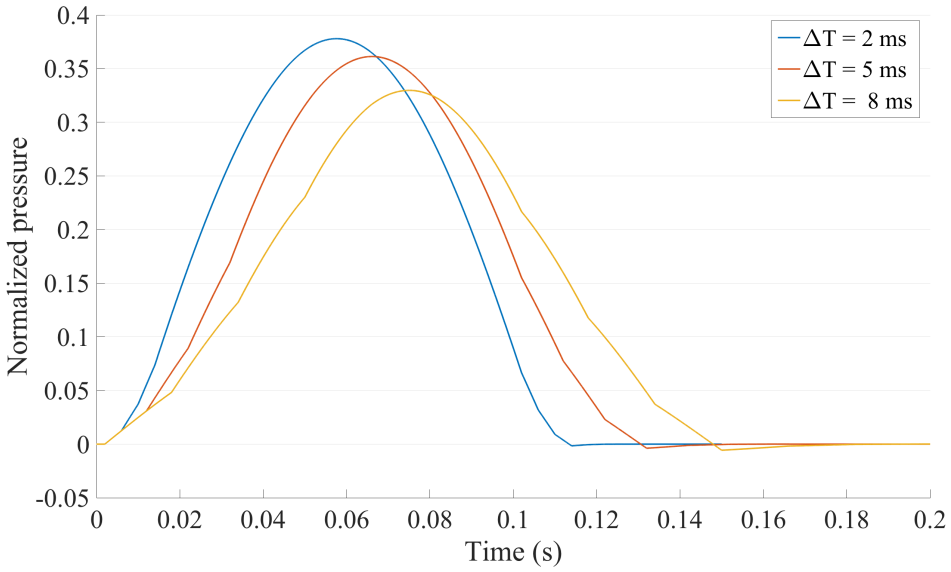

FIGURE 7. Normalized reflected pressure versus time at the entrance of a vessel with a smooth change in stiffness modelled with S_4 for different gradients in stiffness.

needed, limiting the risks and the time of the medical procedure. Our model shows that when two stenoses are in series, the reflected pressure looks similar to the case of isolated stenoses but visible local pressure extrema indicate the presence of the second downstream stenosis. From such information, clinicians could directly look for two stenoses instead of one. However, in practice, noise could easily make the local extrema difficult to measure as their amplitude are relatively small compared to the global amplitude of the reflected pressure wave. This would suppose a measuring device able to detect small pressure variations in the blood flow while filtering undesirable noise. At this point, no experimental work has been done. Yet, from the theoretical results of this research, we understand that an experimental study would need precise measuring tools and techniques in order to detect the impact of such arterial irregularities on the pressure waveform.

Finally we investigate on a progressive change in the vessel's properties. We apply the algorithm on smooth changes in stiffness of the vessel's wall. Results show that the less the gradient stiffness is important, the weaker will be the reflected wave. The limit case of infinitely smooth changes in the vessel's properties being the case of a regular uniform vessel in which no reflected wave is generated. The same method of discretizing progressive changes in the vessel's stiffness can be used to model smooth changes in the vessel's area in order to study more realistic stenoses' and aneurysms' geometries which are commonly modeled by an abrupt change in the vessel's area. However, the main limitation with this discretizing technique is that to have a good approximation of a progressive change in vessels' properties, one need to consider many discontinuities which quickly leads to long computation times.

6. Appendices.

6.1. **Analytical solution of the returning pressure wave for an isolated stenosis or an isolated aneurysm.** In the following we consider a system with two discontinuities S_2 modelling an isolated stenosis or an isolated aneurysm for which $\gamma_{01} = \gamma_{12}$. To ease up the notation we take $\gamma_{01} = \gamma_{12} = \gamma$. We look for the response of S_2 when the incoming pressure wave traveling initially forward through Z_0 is modelled by the Heaviside function H. At time $t = T_0$, it reaches the first discontinuity d_1 of S_2, where a reflected wave is generated with amplitude γ which travels backward to the measurement point M (Figure 1). The reflected wave reaches the measurement point at time $t = 2T_0$. Thus :

$$\forall t \in [0, 2T_0[\quad P_{r,2}(t) = 1. \tag{6.17}$$

When the incoming wave reached d_1 at $t = T_0$ a transmitted wave was also generated, traveling forward through Z_1 with amplitude $1 + \gamma$. When this transmitted wave reaches d_2 at time $t = T_0 + T_1$ a reflected wave is generated, traveling backward through Z_1 with an amplitude of $(1+\gamma)(-\gamma)$ which reaches d_1 at time $T_0 + 2T_1$. At this time a transmitted wave is generated and travels through Z_0 with the amplitude $(1-\gamma^2)(-\gamma)$ and reaches the measurement point at time $t = 2T_0 + 2T_1$. Thus we can write:

$$\forall t \in [2T_0, 2T_0 + 2T_1[\quad P_{r,2}(t) = 1 + \gamma. \tag{6.18}$$

This reflection process within Z_1 goes on infinitely and new waves are transmitted to the measurement points every $2T_1$. Thus we can write:

$$\forall t \in [2T_0 + 2T_1, 2T_0 + 4T_1[\quad P_{r,2}(t) = 1 + \gamma + (1-\gamma^2)(-\gamma) \tag{6.19}$$

and more generally :

$$\forall n \in \mathbb{N}^* \quad \forall t \in [2T_0+2nT_1, 2T_0+2(n+1)T_1[\quad P_{r,2}(t) = 1+\gamma+(1-\gamma^2)\sum_{k=1}^{n}(-\gamma)^{2k-1}. \tag{6.20}$$

By induction we get the general formula for $P_{r,2}(t)$ when the incoming wave is modelled by the Heaviside function H:

$$\forall t \in \mathbb{R}_+^* \quad P_{r,2}(t) = H(t)+\gamma H(t-2T_0)+(1-\gamma^2)\sum_{k=1}^{\infty}(-\gamma)^{2k-1} H\left(t-(2T_0+2kT_1)\right). \tag{6.21}$$

Knowing the response of S_2 for an incoming wave modelled by the Heaviside function, one can know the response of S_2 for any continuous function as explained in section 2.2. From this analytical method we are able to control and validate the results returned by the algorithm for n = 2 (Figure 4).

6.2. **Analysis on the speed of convergence for two discontinuities ($n = 2$) as a function of the reflection coefficient γ.** We know from equation (6.5) the analytical solution of the reflected pressure for $n = 2$, that can be used, for example, to model an isolated stenosis. The first term $H(t)$ represents the input wave that is modelled by the Heaviside side function for the single wavefront analysis developed above. The second term $\gamma H(t - 2T_0)$ comes from the reflection of the input wave before entering in the stenosis. The third and last term $(1-\gamma^2)\sum_{k=1}^{\infty}(-\gamma)^{2k-1} H\left(t-(2T_0+2kT_1)\right)$ describes the multiple reflections and

transmissions occurring within the stenosis. In order to study the asymptotic behavior of $P_{r,2}$ and its speed of convergence, we will study the sequence defined by the last term:

$$\forall N \in \mathbb{N}^* \quad u_N = (1-\gamma^2) \sum_{k=1}^{N} (-\gamma)^{2k-1} . \tag{6.22}$$

The sequence is a geometric series with a common ration of γ. As we saw in the previous part, γ represents the reflection coefficient between Z_0 and Z_1, thus, $\gamma \in [0,1[$ (the case in which $\gamma = 1$ being the trivial case when the stenosis is fully blocked). The fact that $0 \leq \gamma < 1$ indicates that the series converges, as expected. Moreover, as $\gamma \neq 1$, we can rewrite this geometric series as:

$$\forall N \in \mathbb{N}^* \quad u_N = -\gamma \left(1-\gamma^2\right) \frac{1-\left(\gamma^2\right)^N}{1-\gamma^2} = -\gamma \left(1-\gamma^{2N}\right) . \tag{6.23}$$

In order to study the speed of convergence we consider the following sequence :

$$\forall N \in \mathbb{N}^* \quad \Delta u_N = u_N - u_{N-1} = \frac{\left(\gamma^2-1\right)}{\gamma} \gamma^{2N}. \tag{6.24}$$

For $\alpha = \frac{\left(\gamma^2-1\right)}{\gamma}$ we have that :

$$\forall N \in \mathbb{N}^* \quad \Delta u_N = \alpha \cdot \gamma^{2N} = \alpha \cdot e^{2Nln(\gamma)} = \alpha \cdot e^{-\frac{N}{\tau}} \tag{6.25}$$

where,

$$\tau = -\frac{1}{ln\left(\gamma^2\right)} \tag{6.26}$$

is the characteristic number of iterations for convergence that characterizes the speed of convergence. This relation between τ and γ gives us the speed of convergence as a function of γ for two discontinuities (n = 2).

6.3. **Numerical sensitivity analysis of the control parameters m.** The effect of parameter m on the computational solution is clearly visible. As m increases, the computational solution converges towards the analytical solution as expected. On the following Figures, we plotted the same results obtained in Section 4.2, 4.3 and 4.3 but for different values of m. We see that the algorithm converges but a low discretization using Heaviside functions ($m < 1000$) leads to a noisy computational solution. For that matter, we chose in our previous simulations of the results section $m = 10000$.

6.4. **Numerical sensitivity analysis of the control parameter ϵ.**

6.4.1. *Numerical sensitivity analysis of the control parameter ϵ for two discontinuities $n = 2$.* In the case with two discontinuities ($n = 2$), the dynamics of the algorithm convergence can be studied by looking at the evolution of the relative difference between $F_{2,N}[f_m]$ and $F_{2,N-1}[f_m]$, which was previously introduced and denoted $\Delta_r(F_N)$, as a function of the number of iterations N. This evolution is plotted on Figure 11 on which we can see that the algorithm converges after a certain amount of iterations. We also see that the sufficient number of iterations for having $\Delta_r(F_N) < \epsilon$ for a given ϵ, depends on the value of the reflection coefficient γ_{01}. As the reflection coefficient increases, the time for the algorithm to converge is more and more important. Therefore, for the simulations in the results section, we chose the optimal number of iterations for which $\Delta_r(F_N) < \epsilon$ in the case where

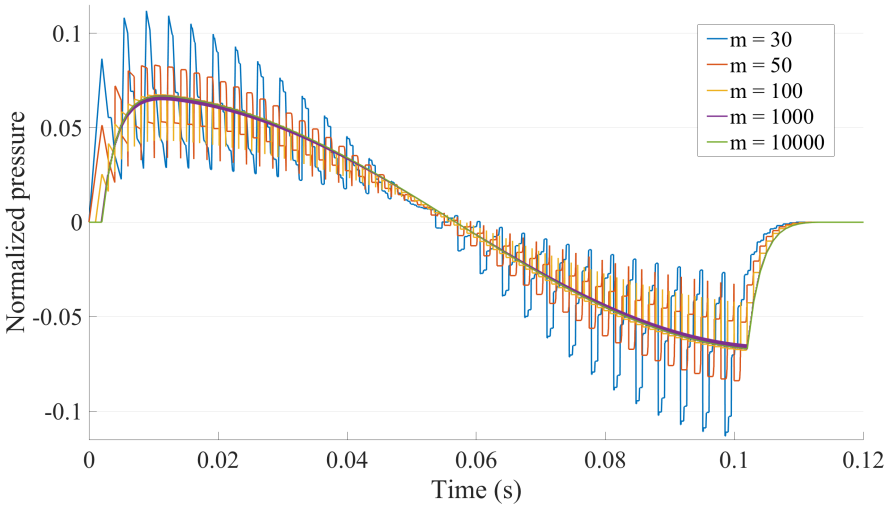

FIGURE 8. Numerical analysis of the effet of the control parameter m on the computational solution in the case of two discontinuities ($n = 2$) with $\gamma_{01} = -\gamma_{12} = 0.8$ as in Section 4.2.

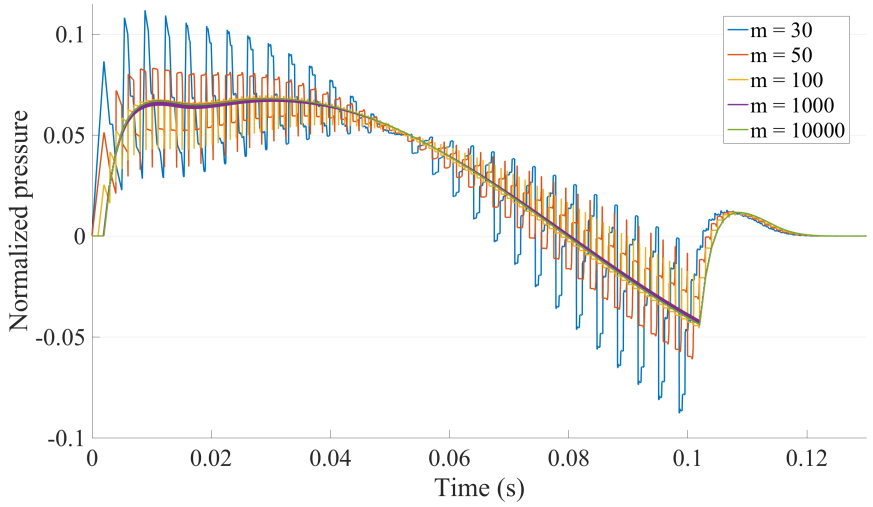

FIGURE 9. Numerical analysis of the effet of the control parameter m on the computational solution in the case of three discontinuities ($n = 3$) with $\gamma_{01} = -\gamma_{12} = 0.8$ and $\gamma_{23} = 0.05$ as in Section 4.3.

$\gamma = 0.8$. Indeed, as $\gamma = 0.8$ is the highest value of the reflection coefficient that we study, its leads to the longest time of convergence and therefore the highest number of iterations. As we chose a control parameter $\epsilon = 0.1$, the simulations were run with the optimal number of iterations which is $N = 12$ in order to optimize computational time and still have a relevant computational solution close to the analytical one. On Figure 12 is plotted the computational solution for different value of the control parameter ϵ. We see that as $\epsilon \to 0$, the computational solution uniformly

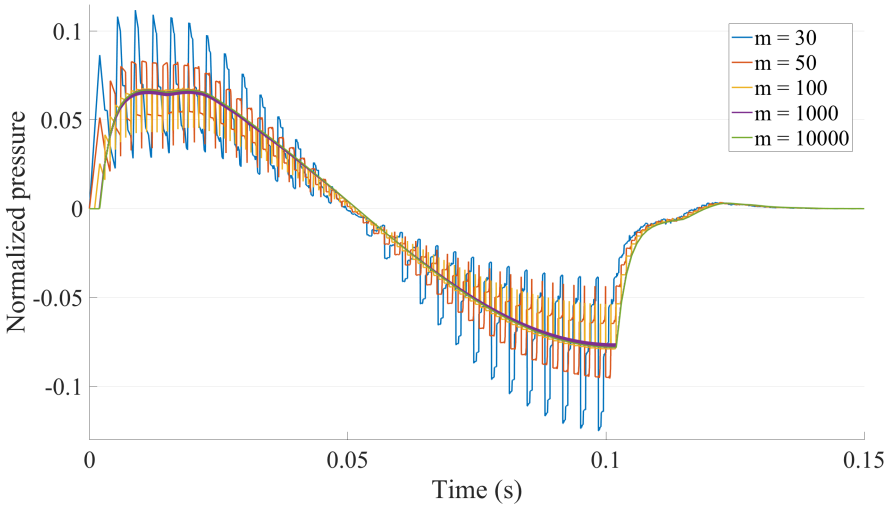

FIGURE 10. Numerical analysis of the effet of the control parameter m on the computational solution in the case of four discontinuities ($n = 4$) with $\gamma_{01} = -\gamma_{12} = 0.8$ and $\gamma_{23} = -\gamma_{34} = 0.2$ as in Section 4.4.

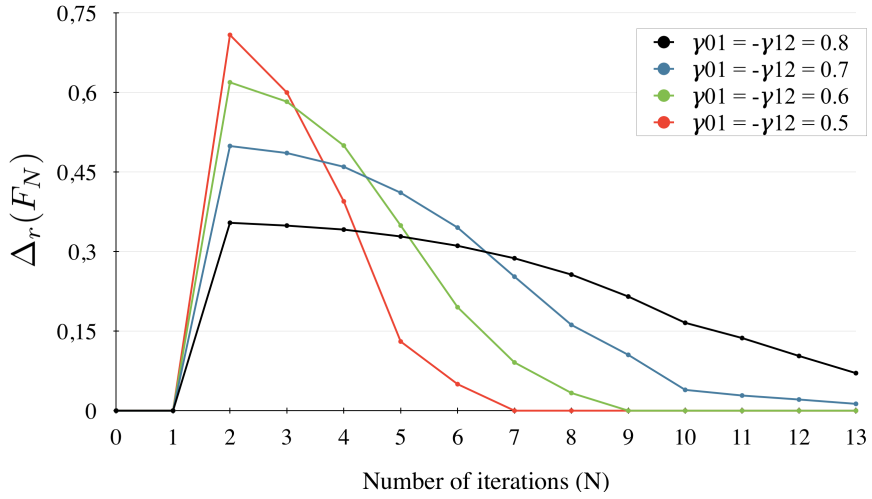

FIGURE 11. Absolute convergence of the computational solution as a function of number of iterations in the case of two discontinuities ($n = 2$) and for different values of reflection coefficients.

converges to the analytical solution, represented in dashed lines in Figure 12, as expected.

6.4.2. *Numerical sensitivity analysis of the control parameter ϵ for more than two discontinuities $n > 2$.* Similarly, numerical sensitivity studies were done for $n = 3$ and $n = 4$ and results are gathered in Figure 13.

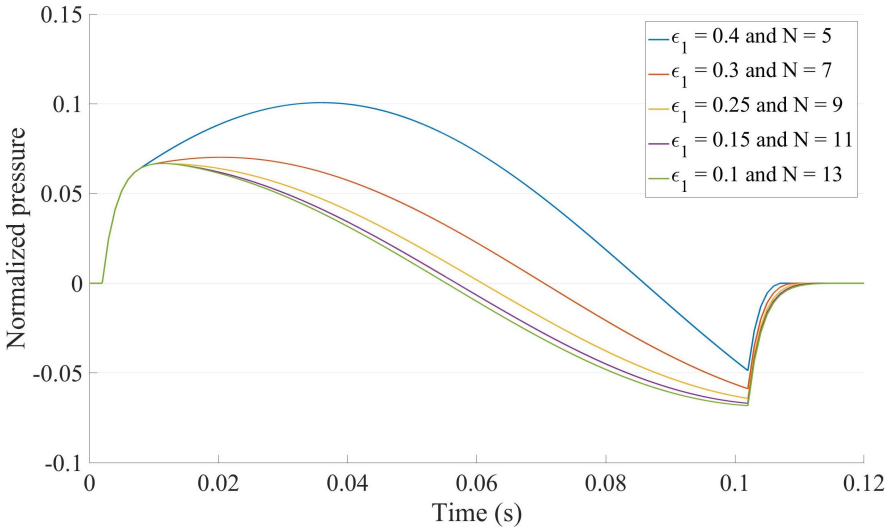

FIGURE 12. Computational solution absolutely converging towards the analytical solution as $\epsilon \to 0$ in the case of two discontinuities ($n = 2$) and $\gamma_{01} = -\gamma_{12} = 0.8$.

REFERENCES

[1] L. Augsburger, P. Reymon, E. Fonck, Z. Kulcar, M. Farhat, M. Ohta, N. Stergiopulos and D. A. Rufenacht, Methodologies to assess blood flow in cerebral aneurysms: Current state of research and perspectives, *Journal of Neuroradiology*, **36** (2009), 270–277.

[2] I. Bakirtas and A. Antar, Effect of stenosis on solitary waves in arteries, *International Journal of Engineering Science*, **43** (2005), 730–743.

[3] W.-S. Duan, Y.-R. Shi, X.-R Hong, K.-P. Lu and J.-B. Zhao, The reflection of soliton at multi-arterial bifurcations and the effect of the arterial inhomogeneity, *Physics Letters A*, **295** (2002), 133–138.

[4] L. Formaggia, F. Nobile, A. Quarteroni and A. Veneziani, Multiscale modelling of the circulatory system: A preliminary analysis, *Comput. Visual. Sci.*, **2** (1999), 75–83.

[5] L. Formaggia, F. Nobile, A. Quarteroni and J.-F. Gerbeau, On the coupling of 3D and 1D Navier-Stokes equations for flow problems in compliant vessels, *Comp. Methods Appl. Mech. Engng.*, **191** (2001), 561–582.

[6] K. Hayashi, K. Handa, S. Nagasawa and A. Okumura, Stiffness and elastic behaviour of human intracranial and extracranial arteries, *J. Biomech.*, **13** (1980), 175–179, 181–184.

[7] G. L. Langewouters, K. H. Wesseling and W. J. A. Goedhard, The static properties of 45 human thoracic and 20 abdominal aortas in vitro and the parameters of a new model, *J. Biomech.*, **17** (1984), 425–435.

[8] C. A. D. Leguy, E. M. H. Bosboom, H. Gelderblom, A. P. G. Hoeks and F. N. Van de Vosse, Estimation of distributed arterial mechanical properties using a wave propagation model in a reverse way, *Medical Engineering & Physics*, **32** (2010), 957–967.

[9] K. S. Matthus, J. Alastruey, J. Peiro, A. W. Khir, P. Segers, R. P. Verdonck, K. H. Parker and S. J. Sherwin, Pulse wave propagation in a model human arterial network: Assessment of 1-D visco-elastic simulations against in vitro measurements, *J. Biomechanics*, **44** (2011), 2250–2258.

[10] H. G. Morales, I. Larrabide, A. J. Geers, M. L. Aguilar and A. F. Frangi, Newtonian and non-Newtonian blood flow in coiled cerebral aneurysms, *J. Biomechanics*, **46** (2013), 2158–2164.

[11] W. W. Nichols, J. W. Petersen, S. J. Denardo and D. D. Christou Arterial stiffness, wave reflection amplitude and left ventricular afterload are increased in overweight individuals, *Artery Research*, **7** (2013), 222–229.

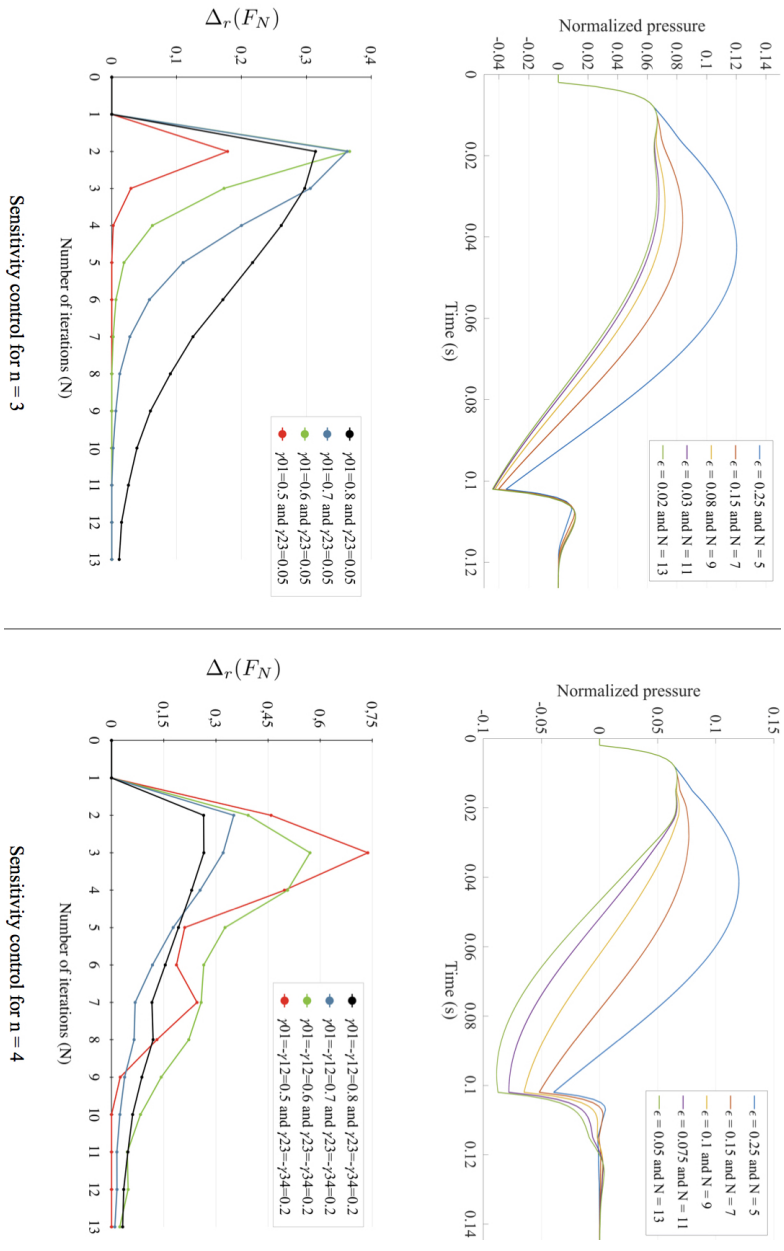

FIGURE 13. (Top) computational solution absolutely converging towards the analytical solution as $\epsilon \to 0$ for (left) n = 3 with $\gamma_{01} = -\gamma_{12} = 0.8$ and $\gamma_{23} = 0.05$ and for (right) n = 4 with $\gamma_{01} = -\gamma_{12} = 0.8$ and $\gamma_{23} = -\gamma_{34} = 0.2$ and (bottom) $\Delta_r(F_N)$ convergence as the number of iterations increases for (left) $n = 3$ and (right) $n = 4$ for different values of reflection coefficients.

[12] Z. Ovadia-Blechman, S. Einav, U. Zaretsky, D. Castel and E. Eldar, Characterization of arterial stenosis and elasticity by analysis of high-frequency pressure wave components, *Computer in Biology and Medicine*, **33** (2003), 375–393.
[13] C. S. Park and S. J. Payne, Nonlinear and viscous effects on wave propagation in an elastic axisymmetric vessel, *J. of Fluids and Structures*, **27** (2011), 134–144.
[14] K. H. Parker, An introduction to wave intensity analysis, *Medical & Biological Engineering & Computing*, **47** (2009), 175–199.
[15] T. J. Pedley, Nonlinear pulse wave reflection at an arterial stenosis, *J. of Biomechanical Engineering*, **105** (1983), 353–359.
[16] S. I. S. Pinto, E. Doutel, J. B. L. M. Campos and J. M. Miranda, Blood analog fluid flow in vessels with stenosis: Development of an Openfoam code to stimulate pulsatile flow and elasticity of the fluid, *APCBEE Procedia*, **7** (2013), 73–79.
[17] A. Quarteroni and L. Formaggia, Mathematical modelling and numerical simulation of the cardiovascular system, *Handbook of Numerical Analysis*, **12** (2004), 3–127.
[18] P. Segers, J. Kips, B. Trachet, A. Swillens, S. Vermeersch, D. Mahieu, E. Rietzschel, M. D. Buyzere and L. V. Bortel, Limitations and pitfalls of non-invasive measurement of arterial pressure wave reflections and pulse wave velocity, *Artery Research*, **3** (2009), 79–88.
[19] D. Shahmirzadi and E. E. Konofagou, Quantification of arterial wall inhomogeneity size, distribution, and modulus contrast using FSI numerical pulse wave propagation, *Artery Research*, **8** (2014), 57–65.
[20] N. Stergiopulos, D. F. Young and T. R. Rogge, Computer simulation of arterial flow with applications to arterial and aortic stenoses, *J. Biomechanics*, **25** (1992), 1477–1488.
[21] N. Stergiopulos, F. Spiridon, F. Pythoud and J. J. Meister, On the wave transmission and reflection properties of stenoses, *J. Biomechanics*, **29** (1996), 31–38.
[22] A. Swillens and P. Segers, Assessment of arterial pressure wave reflection: Methodological considerations, *Artery Research*, **2** (2008), 122–131.
[23] A. Tozeren, Elastic properties of arteries and their influence on the cardiovascular system, *J. Biomech. Eng.*, **106** (1984), 182–185.
[24] C. Tu, M. Deville, L. Dheur and L. Vanderschuren, Finite element simulation of pulsatile flow through arterial stenosis, *J. Biomechanics*, **25** (1992), 1141–1152.
[25] J. J. Wang and K. H. Parker, Wave propagation in a model of the arterial circulation, *J. Biomechanics*, **37** (2004), 457–470.

Received December 24, 2016; Accepted January 23, 2018.

E-mail address: alexandre.cornet@ens-paris-saclay.fr